Journal of Materials Chemistry A

Accepted Manuscript

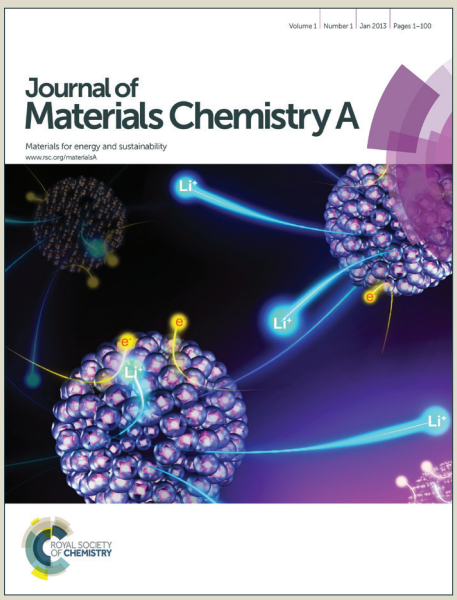

ROYAL SOCIETY OF CHEMISTRY

www.rsc.org/materialsA

Journal Name

RSCPublishing

ARTICLE

Excellent Electrochemical Performance of $LiFe_{0.4}Mn_{0.6}PO_4$ Microspheres Produced Using Double Carbon Coating Process

Cite this: DOI: 10.1039/x0xx00000x

Received 00th January 2012,
Accepted 00th January 2012

DOI: 10.1039/x0xx00000x

www.rsc.org/

Yong Ping Huang,[a] Tao Tao,[b] Zheng Chen,[a] Wei Han,[c] Ying Wu,[a] Chunjiang Kuang,[a] Shaoxiong Zhou[a] and Ying Chen*[b]

Composite $LiFe_{0.4}Mn_{0.6}PO_4$/C microspheres are considered advanced cathode materials for electric vehicles and other high-energy density applications due to the advantages of high energy density and excellent cycling stability. $LiFe_{0.4}Mn_{0.6}PO_4$/C microspheres have been produced using a double carbon coating process employing traditional industrial techniques (ball milling, spray-drying and annealing). The obtained $LiFe_{0.4}Mn_{0.6}PO_4$ microspheres exhibit a high discharge capacity of around 166 mAh g^{-1} at 0.1 C and excellent rate capabilities of 132, 103, and 72 mAh g^{-1} at 5, 10, and 20 C, respectively. A reversible capacity of about 152 mAh g^{-1} after 500 cycles at a current density of 1 C indicates an outstanding cycling stability. The excellent electrochemical performance is attributed to the micrometer-sized spheres of double carbon-coated $LiFe_{0.4}Mn_{0.6}PO_4$ nanoparticles with improved electric conductivity and higher Li ion diffusion coefficients, ensuring full redox reactions of all nanoparticles. The results show that the advanced high-energy density cathode materials can be produced using existing industry techniques.

Introduction

Lithium manganese phosphate ($LiMnPO_4$) has a high working potential of 4.1 V vs Li^+/Li compared to 3.5 V vs Li^+/Li of $LiFePO_4$, [1-3] and thus can provide 20% more energy density than $LiFePO_4$ for lithium ion batteries, and are thus suitable for high energy density applications such as electric vehicles and hybrid cars. However, its lower electrical and ionic conductivities cause poor discharge capacity and rate capacity.[4,5] This issue can be improved by substituting some Mn ions with Fe ions to form a solid solution $LiFe_{1-x}Mn_xPO_4$ in the region of $0 \leq x \leq 0.8$.[6-10] For example, $LiFe_{0.4}Mn_{0.6}PO_4$ is one of the most promising cathode materials due to its high theoretical capacity ($\sim$170 mAh g^{-1}) and higher operating voltages of 3.5-4.1V.[2,11] Large-scale production at low cost is crucial for real commercialization of this cathode material. Recently, various processes have been developed to produce $LiFe_{1-x}Mn_xPO_4$ with different structures. Micrometer-sized spherical structures consisting of carbon-coated, nano-sized primary crystallites are appealing, because micrometer-sized spherical particles pack well and are easy to handle during electrode industry manufacturing.[12-15] Moreover, this porous spherical structure increases the interfacial area with electrolyte, allowing fast charge transport and improves rate capability. The three-dimensional carbon networks between nanoparticles of active materials can significantly enhance the electronic conductivity, and prevent aggregations of active material during cycling. The synthesis of $LiFe_{1-x}Mn_xPO_4$ microspheres have been reported using several advanced techniques including co-precipitation,[10,16-18] sol-gel,[19-23] hydrothermal,[12,24-29] double carbon coating,[8,30,31] and high-energy ball milling.[32,33] Some of them need to be scaled up for mass production.

In this study, traditional processing techniques (i.e. ball milling, spraying and thermal annealing widely used in industry for $LiFePO_4$ production) were used to produce an excellent cathode material ($LiFe_{0.4}Mn_{0.6}PO_4$/C microspheres) with excellent electrochemical performance. A systematic study has been conducted to investigate the microsphere formation and carbon coating process in order to optimise the electrochemical performance. A large range of analyses on single and double coated samples were conducted to reveal the relationship between carbon coating layers and final electrochemical behaviours.

Experimental

Synthesis of $LiFe_{0.4}Mn_{0.6}PO_4$/C microspheres

Stoichiometric amounts of $Li_2C_2O_4$ (99%, Alfa), $FeC_2O_4 \cdot 2H_2O$(99%, Alfa), $MnC_2O_4 \cdot 2H_2O$ (99%, Alfa) and $NH_4H_2PO_4$(98%, Alfa) were ball milled in a planetary mill (Fritsch-P5) with a zirconia container at a rotation speed of 300 rpm in air at room temperature for 40 hours to prepare a precursor. The weight ratio of the zirconia ceramic balls to the raw materials was 10:1. At the end of 40 hours of milling, 1 g of glucose and 250 ml of ethanol were added into the mill, and the mixture was ball milled again for 5 hours to produce homogenous slurry, which was then dried using a spray-drying

process to produce fine and dispersed particles. The fine particles were annealed at 500 °C for 5 hours under an Ar/H_2 (5% H_2) gas flow to produce the first carbon-coated $LiFe_{0.4}Mn_{0.6}PO_4$. The annealed sample (18 g) was mixed with glucose (1 g) and ethanol (250 ml) in the mill and milled for another 5 hours for second carbon coating. The new slurry was spray-dried, and annealed at 600 °C for 10 hours under Ar/H_2 (5% H_2) gas flow to produce the final double carbon-coated samples. The preparation procedure is illustrated in Fig. 1a. For comparison purpose, the single carbon-coated sample was also prepared (Fig. 1b). The difference is that 2 grams of glucose were used once only before the final annealing at 600 °C, which is a common practice in industry.

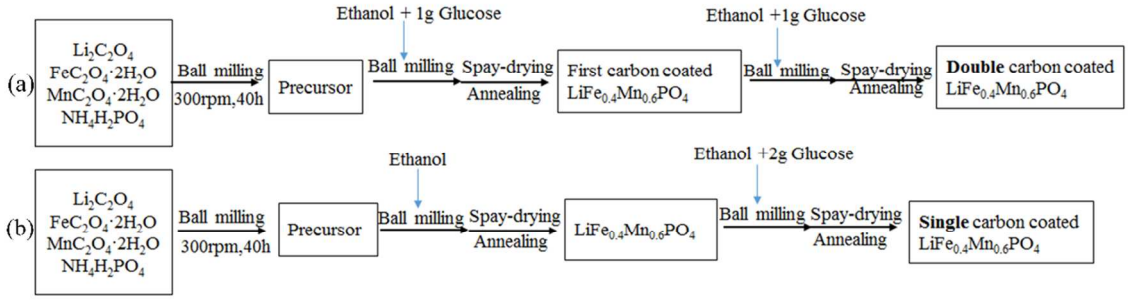

Fig.1 Schematic production processes of (a) double and (b) single carbon-coated $LiFe_{0.4}Mn_{0.6}PO_4$.

Materials characterization

X-ray powder diffraction (XRD) analysis was performed with a BrukerD8 Discover diffractometer using Cu Kα radiation (40 kV, 40 mA). A 2ɵ survey scan was performed from 15° to 125° with a step size of 0.02° and step time of 2 seconds. The lattice parameters were refined using the Rietveld analysis with the Fullprof software. Scanning electron microscopy (SEM) and transmission electron microscopy (TEM) images were obtained using FEI-Nova Nano-SEM450 and JEOL JEM2100F systems, respectively. The surface area was measured using the Brunauer-Emmet-Teller (BET) method with a QuantaAutosorb-iQ2-MP-ANG-VP instrument. The carbon content was determined using a high frequency infrared Carbon-sulfur analyser (ELTRA, CS800). Thermal gravimetric analyser (TGA) (NETZSCH, STA 449F3, N_2, 5 $Kmin^{-1}$, 40 $mlmin^{-1}$) was used to monitor the thermal decomposition process of samples. Raman spectroscopy characterization was performed using a LabRAM HR800 instrument from HORIBA JOBIN YVON S.A.S. with a laser of 532.15 nm and a power at 50 mW.

Electrochemical characterization

The electrochemical properties were measured in CR2025 coin-type cells, which were assembled in an argon-filled glove box. The prepared material was used as the cathode electrode, metallic lithium foil as the counter electrode, Celgard-2400 membrane as the separator, and a mixture of 1 M $LiPF_6$ in a 1:1 ethylene carbonate (EC) and dimethyl carbonate(DMC) as the electrolyte. The cathode electrodes were prepared by mixing the active materials (sample, 85 wt%) with carbon black (10 wt%), and polyvinylidene fluoride (PVDF, binder, 5 wt%) in N-methylpyrrolidone (NMP) to form homogenous slurry. The slurry was spread onto an aluminium current collector and dried at 110 °C for 20 hours in a vacuum oven. The electrode foils were pressed and cut into circular strips to have the material loading of about 2 mg cm^{-2}. The cells were galvanostatically charged–discharged at various current rates between 2.0 and 4.5 V vs. Li/Li^+ using LAND battery system (CT2001A, Wuhan LAND Electronics, Ltd. China). The cyclic voltammetry measurement of the cells was performed under different sweep rates over the same voltage range using a Bio-Logic VMP3 instrument. The cells were activated twice at a current density of 0.1 C (all C rates based on the theoretical specific capacity of $LiFe_{0.4}Mn_{0.6}PO_4$, where a 1 C rate corresponds to a current density of 170 mAg^{-1}). The electrochemical impedance spectroscopy (EIS) was also performed in the frequency range between 1 MHz and 1 mHz with amplitude of 5 mV with the same Bio-Logic VMP3 instrument.

Results and discussion

Fig. 2a shows the XRD pattern and Rietveld refinement of the double carbon-coated sample. All the diffraction peaks can be indexed into an orthorhombic olivine structure. The structural parameters of the unit cell are given in supplementary information (Table S1, supplementary information) and the corresponding lattice parameters (a, b, c, and V) are 10.4060(4) Å, 6.0663(2) Å, 4.7253(2) Å, and 298.29(2) Å, respectively, which is in agreement with the $LiFe_{0.4}Mn_{0.6}PO_4$ phase reported in ref. 2.

Actually, the $LiFe_{0.4}Mn_{0.6}PO_4$ phase might have been formed after the first carbon coating and pre-annealing treatment as the corresponding XRD pattern (Fig. S1, supplementary information) reveals. The in-situ first carbon coating treatment prevents the formation of large-sized crystals and also improves the conductivity of the $LiFe_{0.4}Mn_{0.6}PO_4$. For comparison, the XRD pattern of the single carbon-coated sample is displayed in Fig. 2b. The similar XRD patterns of the single and double carbon-coated samples

reveal the same olivine-type structure (PDF No. 40-1499) which were formed in both cases because of the same annealing conditions used.

Raman spectroscopy was applied to analyze the structure of the in-situ formed carbon coating, and the Raman spectra are shown in the supplementary information Fig. S2. Two broad bands at 1356 and 1601 cm^{-1} are attributed to the disordered structure (D-band) and six-member rings (G-band), respectively. The similar spectra show no major difference between the crystalline structure of the single and double coated carbon layers. The carbon content of the single coated sample is 3.8 wt%, coming from 2 g of glucose. For the double carbon coated sample, one gram of glucose was used in the first coating treatment, which gives the carbon content of 1.98 wt%, the second coating with another 1 g of glucose leads to the final content of 3.7 wt%. Therefore, both samples have similar C contents.

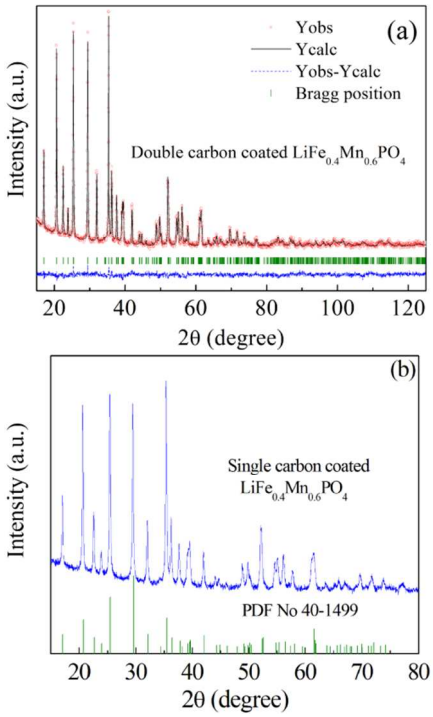

Fig. 2 Rietveld refinement of the XRD patterns of the double (a) and single (b) carbon coated $LiFe_{0.4}Mn_{0.6}PO_4$.

Fig. 3a shows a typical low-magnification SEM image of the double carbon-coated $LiFe_{0.4}Mn_{0.6}PO_4$. Micrometer-sized spheres with a uniform size distribution in the range of 3-10 μm can be seen throughout the sample. The high-magnification SEM image in Fig. 3b shows one individual microsphere composed of a large number of nanometer-sized particles. The TEM image (Fig. 3c) reveals that the nanoparticles are covered and connected by carbon layers. A high resolution TEM image (Fig. 3d) of one nanoparticle shows a well-crystallized structure, oriented along the [010] and [100] zone axis. The indexed fast Fourier transform (FFT) pattern in Fig. 3e shows crystal planes with a d-spacing of 0.30 nm and 0.52 nm, corresponding to the (020) and (200) planes of $LiFe_{0.4}Mn_{0.6}PO_4$ calculated from the previous XRD results. The [010] axis is generally considered as the Li^+ diffusion channel direction in $LiFe_{0.4}Mn_{0.6}PO_4$ crystals (Fig. 3f).[4, 34]

SEM and TEM images of single carbon-coated $LiFe_{0.4}Mn_{0.6}PO_4$ are shown in Fig. 4. The sample consists of predominantly sub-micrometer-sized, irregular-shaped agglomerates of nanoparticles. The TEM image in Fig. 4b reveals the small particles of a typical size ranging from several to tens of nanometres. Some $LiFe_{0.4}Mn_{0.6}PO_4$ nanoparticles are not covered by carbon layer (Fig. 4b), suggesting single carbon coating treatment may not be efficient to cover every $LiFe_{0.4}Mn_{0.6}PO_4$ nanoparticle, although double amount of carbon source (2 g of glucose) was used.

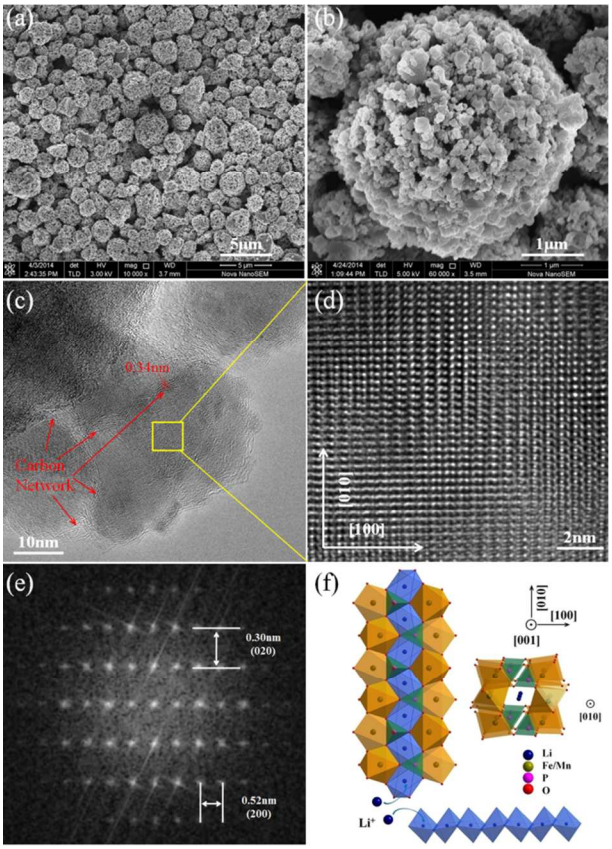

Fig. 3 SEM and TEM images of the double carbon-coated $LiFe_{0.4}Mn_{0.6}PO_4$: (a) low and (b) high-magnification SEM images; (c) and (d) typical TEM images for $LiFe_{0.4}Mn_{0.6}PO_4$/C particles containing several primary crystallites, (e) FFT pattern of the lattice structure in (d), and (f) representation of the crystal structure of $LiFe_{0.4}Mn_{0.6}PO_4$.

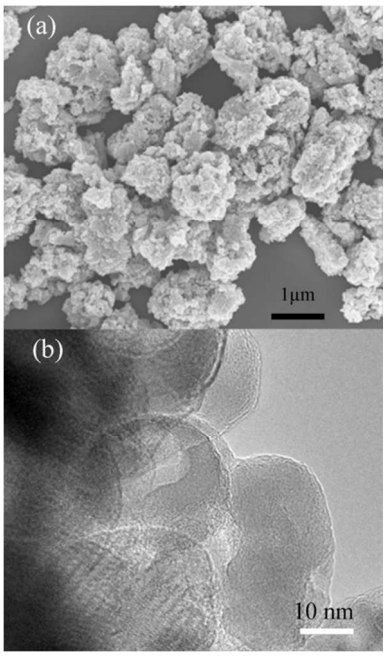

Fig. 4 (a) SEM and (b) TEM images of the single carbon-coated $LiFe_{0.4}Mn_{0.6}PO_4$.

Nitrogen adsorption/desorption isotherms and Barrett-Joyner-Halenda (BJH) pore-size distribution curves of the single and the double carbon-coated $LiFe_{0.4}Mn_{0.6}PO_4$ are shown in supplementary information Fig. S3. The small hysteresis in nitrogen adsorption/desorption isotherms shown in Fig. S3a, c reveals a mesoporous structure for the single (Fig. S3a) and the double (Fig.S3c) carbon-coated $LiFe_{0.4}Mn_{0.6}PO_4$, respectively. The BJH curves (Fig.S3b, S3d) show the double carbon-coated sample has a narrow pore size distribution (1-10nm) (Fig. S3d). The single coated sample has a pore size distribution in the range of 4-40nm.

The pore volume of the single carbon-coated sample is higher than that of the double carbon-coated sample. The corresponding BET surface area of the single carbon-coated sample is 43 m^2 g^{-1}, which is slightly higher than that of the double coated sample (37 m^2 g^{-1}). The different pore-size distributions, surface areas, as well as different morphologies (Fig. 3b and 4a) may suggest that the nanoparticles were not well connected by carbon coating in the single-coated samples and the double carbon coating connects all nanoparticles forming micrometer-sized spheres with a higher density.

Fig. 5 compares the electrochemical performance of the single and double carbon-coated $LiFe_{0.4}Mn_{0.6}PO_4$ electrodes. Fig. 5a shows the initial charge and discharge curves of the electrodes at the rate of 0.1 C. The electrode of the double carbon sample delivers a very high discharge capacity of about 165.8 mAh g^{-1}, which is just under its theoretical capacity of 170 mAh g^{-1}, and this value is among the best discharge capacities obtained from the microspheres produced using other techniques.[8, 35, 36] Both the discharge and charge curves have two voltage plateaus at about 3.5 V and 4.1 V, corresponding to the $Fe^{2+/3+}$ (3.5 V) and $Mn^{2+/3+}$(4.1 V) redox couples. The capacity ratio of the 3.5 V plateau ($Fe^{2+/3+}$, 71.9 mAh g^{-1}) to the 4.1 V plateau ($Mn^{2+/3+}$, 93.9 mAh g^{-1}) is 0.43: 0.57, closing to the Fe/Mn ratio in $LiFe_{0.4}Mn_{0.6}PO_4$, indicating full contribution from Fe and Mn redox reactions and most likely all nanoparticles are involved in the charge/discharge processes.

In the case of single carbon coated sample, the 3.5 V ($Fe^{2+/3+}$) plateau gives the capacity of 64.5 mAh g^{-1} and the 4.1 V ($Mn^{2+/3+}$) plateau delivers 64.1 mAh g^{-1}, the total capacity is 128.6 mAh g^{-1}, much lower than that of double coated sample; the capacity ratio is about 0.5:0.5, which is higher than the Fe/Mn ratio, implying some nanoparticles may not participate the redox reactions possibly lack of carbon coating. Because of higher energy barrier, the $Mn^{2+/3+}$ reactions may be more difficult to be activated than the $Fe^{2+/3+}$ reactions in the case of poor conductivity.[4]

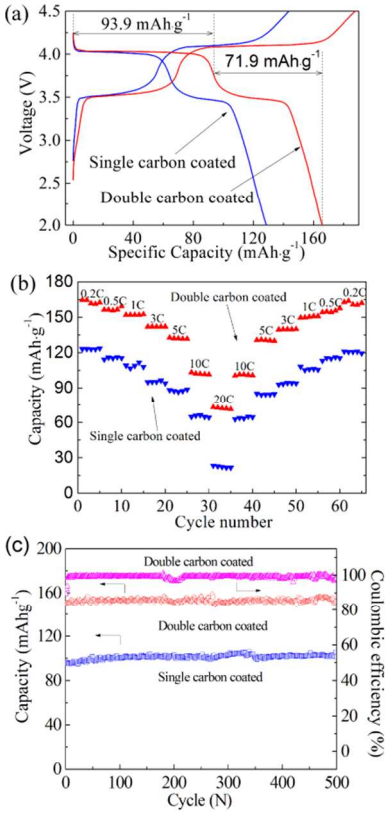

Fig. 5 Comparison of electrochemical performance between the double and single carbon coated $LiFe_{0.4}Mn_{0.6}PO_4$: (a) the first charge/discharge curves at a current density of 0.1 C, (b) rate capability, and (c) cycling performance at a current density of 1 C.

Fig. 5b shows an impressive rate capability of the double coated electrodes, which delivers a higher discharge capacity of 164.5 mAh g^{-1} at a current rate of 0.2 C, and remains high at 132 mAh g^{-1} at 5 C and 103 mAh g^{-1} at 10 C. Even at a rate of 20 C, it can still deliver a discharge capacity of 72 mAh g^{-1}. When the current density is returned back to 0.2 C, a discharge capacity of 162 mAh g^{-1} is recovered, indicating a stable structure. Single carbon-coated sample has lower rate capacities at all tested current densities (corresponding capacities of 123, 88, 65 and 22mAh g^{-1} at current rates of 0.2, 5, 10 and 20 C, respectively). Fig. 5b shows the differences between each rate capacities of the two samples are about same, which may suggest both samples have the same rate capacities under different discharge capacity levels, and the different carbon coating or morphology do not give any effect under high current rates. Sun *et al*[36] also found the microsphere structures deliver a higher discharge capacity but do not improve the rate capacities compared with loose nanoparticles.

Fig. 5c compares the discharge/charge cycling stability of the single and double carbon-coated $LiFe_{0.4}Mn_{0.6}PO_4$ electrodes. Stable discharge capacities of about 152 and 101mAh g^{-1} are obtained after 500 cycles at 1 C rate for the double and single carbon-coated electrodes, respectively. The almost flat curves show both samples have excellent cycling stability, possibly due to the good crystalline structure of $LiFe_{0.4}Mn_{0.6}PO_4$ in both samples. Again, no influence can be seen from different carbon coating treatment. The Coulombic efficiency of the double carbon-coated electrode remains above 98% after the third cycle.

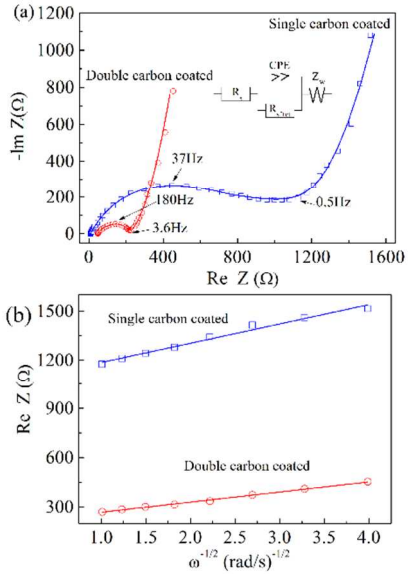

Fig.6. Electrochemical impedance spectra (a) and the plots of the real part of impedance as a function of the inverse square root of angular frequency (b) for the double and single carbon coated $LiFe_{0.4}Mn_{0.6}PO_4$

Fig. 6a presents the Nyquist plots of the single and double carbon-coated $LiFe_{0.4}Mn_{0.6}PO_4$ electrodes. The inset in Fig. 6a shows an equivalent circuit to simulate the electrochemical impedance data. R_s represents the ohmic resistance, and R_{sf+ct} stands for the related charge-transfer resistance. CPE and Z_w stand for the constant phase element and the Warburg diffusion impedance, respectively. It is clearly seen that the R_{sf+ct} value of the double coated electrode (175.5Ω) is much smaller than that of the single coated electrode (924.9Ω). The diffusion coefficient of Li ions in the electrode can be calculated from the low frequency Warburg impedance.[37] Fig.6b shows the relationship between R_c (Z) and the inverse square root of angular frequency in the low frequency range. The diffusion coefficient of lithium ions in the single coated electrode was calculated to be 7.1×10^{-14} cm^2 s^{-1}, which is lower than that of the double coated electrode (2.6×10^{-13} cm^2 s^{-1}). Therefore the electrons can transfer more quickly in the double coated structure. Both samples have similar amount of carbon but the different conductivities, maybe because of different distribution or coverage of carbon coating over $LiFe_{0.4}Mn_{0.6}PO_4$ nanoparticles.

Fig. 7 shows the CV curves of the double and single carbon-coated $LiFe_{0.4}Mn_{0.6}PO_4$/C electrodes at different scan rates from 0.01 mV s^{-1} to 0.1 mV s^{-1}.The cathodic peaks shift to high potential and the anodic peaks shift to low potential with increasing scan rate. The peak current (i_p) shows a good linear relation with the square root of scanning rate ($v^{1/2}$). From these profiles, the chemical diffusion coefficient of Li ion in $LiFe_{0.4}Mn_{0.6}PO_4$/C microsphere can be calculated via the Randles–Sevcik equation from the slope of i_p as a function of $v^{1/2}$:[38]

$$i_P = 2.69\times10^5 n^{3/2} A D_{Li}^{1/2} v^{1/2} \Delta C_0 \quad (1)$$

Where i_p is the peak current (A), n is the charge transfer number, A is the surface area of electrodes (cm^2), D is the diffusion coefficient (cm^2 s^{-1}) measured by CV, v is the scanning rate (V s^{-1}), and ΔC_0 is the concentration of reaction. The cathodic and anodic diffusion constants of Fe^{2+}/Fe^{3+} in the double carbon coated $LiFe_{0.4}Mn_{0.6}PO_4$/C microsphere system are calculated to be 2.5×10^{-11} cm^2 $s^{-1}$and 1.5×10^{-11} cm^2 s^{-1}, and Mn^{2+}/Mn^{3+} to be 3.9×10^{-11} cm^2 s^{-1} and 5.5×10^{-11} cm^2 s^{-1}, respectively. The cathodic and anodic diffusion constant of Fe^{2+}/Fe^{3+} in the single carbon coated system are 1.1×10^{-11} cm^2 s^{-1} and 2.4×10^{-11} cm^2 s^{-1}, and Mn^{2+}/Mn^{3+} are 2.0×10^{-11} cm^2 s^{-1} and 5.5×10^{-12} cm^2 s^{-1}, respectively. Consequently, the Li ion diffusion coefficient of the double carbon-coated $LiFe_{0.4}Mn_{0.6}PO_4$ is higher than that of the single carbon-coated $LiFe_{0.4}Mn_{0.6}PO_4$.

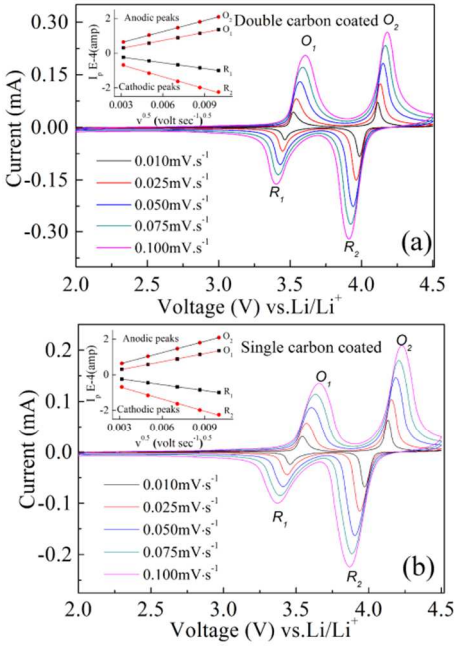

Fig. 7 CV curves of the double (a) and single (b) carbon-coated $LiFe_{0.4}Mn_{0.6}PO_4$. inset: the diffusion coefficients of lithium-ion calculated from CV curves.

The chemical diffusion coefficients of the single and double carbon coated electrode have been evaluated by both CV and EIS techniques as described above. Although different Li ion chemical diffusion coefficients of the double carbon coated $LiFe_{0.4}Mn_{0.6}PO_4$ were obtained (about 6.4×10^{-11} cm^2 s^{-1} from CV and 2.6×10^{-13} cm^2 s^{-1} from EIS), the diffusion coefficients of the double carbon-coated samples are higher than those of the single coated samples using both methods, indicating better intrinsic kinetic property of the electrode material.[39]

As shown in Fig. 8, each nanoparticle of $LiFe_{0.4}Mn_{0.6}PO_4$ has an almost single-crystal structure (as TEM image shows) and thus Li^+ ion intercalation takes place only at certain directions because Li^+ ions diffuse along the [010] directions. Because of lack of carbon layer, the electrons cannot reach all the positions where Li^+ ion intercalation takes place, and these particles don't contribute to the electron charge and discharge. Full carbon coating on every particle ensures all particles get electrons from all directions, and open surface is also needed to allow Li ions to diffuse into these channels. In the single coated sample, some nanoparticles are not coated by carbon layers, so they do not contribute to the storage, resulting to a lower charge/discharge capacities as well as rate capacities. In addition, the lower electrical and ionic conductivities of $LiFe_{0.4}Mn_{0.6}PO_4$ particles without carbon coating (9.0×10^{-17} cm^2 s^{-1}) results in poor electrochemical performances (Fig. S4). The electrode without carbon coating only delivers a discharge capacity of 21.4 mAh g^{-1} at a current rate of 0.1 C, and its capacity drops quickly (2.5 mAh g^{-1}) when the current rate reaches 0.2 C. These results suggest suitable carbon coating of nanoparticles of active materials is critical.

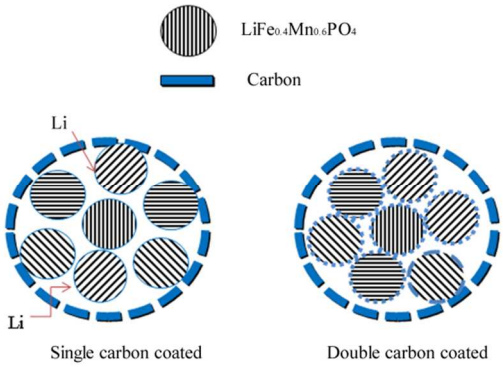

Fig. 8. Schematic structures of the single and double carbon coated $LiFe_{0.4}Mn_{0.6}PO_4$.

Conclusions

A remarkable cathode material of $LiFe_{0.4}Mn_{0.6}PO_4$/C microspheres have been produced via a double carbon coating process, which establishes a 3D carbon network between $LiFe_{0.4}Mn_{0.6}PO_4$ nanoparticles, ensuring most particles contribute to electron charge/discharge. The microspheres exhibit excellent electrochemical performance with high capacity, impressive rate capability and good cycling life. The specific capacity of the $LiFe_{0.4}Mn_{0.6}PO_4$/C microsphere is 165.8 mAh g^{-1} at a rate of 0.1 C, and reached

132, 103, and 72 mAh g^{-1} at 5 C, 10 C, and 20 C, respectively. A high reversible capacity of 152 mAh g^{-1} at 1 C has been obtained after 500 cycles. The results demonstrate outstanding cathode materials can be produced using industrial techniques by fine designing/tuning operation conditions. The use of glucose as the carbon source further reduces the production cost. The double coating process discovered in this study can be directly applied to current industrial cathode material production process for mass production of high-energy density cathode materials for Li-ion batteries.

Acknowledgements

This work is greatly supported by Advance Technology & Materials Co., Ltd Innovation Foundation (Grant no. 2011JA01GYF, Grant no. 2011JA02GYF and Grant no. 2013JA02PYF), China Iron & steel Research Institute Group Foundation (Grant no. SHI11AT0540A).

Notes and references

[a] China-Australia Energy Nanomaterials Joint Research Centre, Advance Technology & Materials Co., Ltd, China Iron & steel Research Institute Group, Beijing 100081, P.R. China.

[b] Institute for Frontier Materials, Deakin University, Waurn Ponds, Victoria 3216, Australia. Fax: +61 3 52271103; Tel: +61 3 52273243; E-mail: ian.chen@deakin.edu.au.

[c] China Iron & steel Research Institute Group, Beijing 100081, P.R. China.

1 A.K. Padhi, K.S. Nanjundaswamy, J.B. Goodenough, *J. Electrochem. Soc.*, 1997, **144**, 1188.
2 A. Yamada, Y. Kudo, K.Y. Liu, *J. Electrochem. Soc.*, 2001, **148**, A747.
3 V. Aravindan, J. Gnanaraj, Y.S. Lee, S. Madhavi, *J. Mater. Chem. A*, 2013, **1**, 3518.
4 S.P. Ong, V.L. Chevrier, G. Ceder, *Phys. Rev. B*, 2011, **83**, 075112.
5 S.L. Shang, Y. Wang, Z.G. Mei, X.D. Hui, Z.K. Liu, *J. Mater. Chem.*, 2012, **22**, 1142.
6 S.K. Martha, J. Grinblat, O. Haik, E. Zinigrad, T. Drezen, J.H. Miners, I. Exnar, A. Kay, B. Markovsky, D. Aurbach, *Angew. Chem. Int. Ed.*, 2009, **48**, 8559.
7 H.L. Wang, Y. Yang, Y.Y. Liang, L.F. Cui, H.S. Casalongue, Y.G. Li, G.S. Hong, Y. Cui, H.J. Dai, *Angew. Chem. Int. Ed.*, 2011, **50**, 7364.
8 W. Liu, P. Gao, Y.Y. Mi, J.T. Chen, H.H. Zhou, X.X. Zhang, *J. Mater. Chem. A*, 2013, **1**, 2411.
9 Y.J. Zhong, J.T. Li, Z.G. Wu, X.D. Guo, B.H. Zhong, S.G. Sun, *J. Power Sources*, 2013, **234**, 217.
10 S.M. Oh, S.T. Myung, Y.S. Choi, K.H. Oh, Y.K. Sun, *J. Mater. Chem.*, 2011, **21**, 19368.
11 J.L. Liu, W.J. Liao, A.S. Yu, J. Alloys Compd., 2014, **587**, 133-137.
12 C.W. Sun, S. Rajasekhara, J.B. Goodenough, F. Zhou, *J. Am. Chem. Soc.*, 2011, **133**, 2132.
13 Y.Z. Wang, X. Shao, H.Y. Xu, M. Xie, S.X. Deng, H. Wang, J.B. Liu, H. Yan, *J. Power Sources*, 2013, **226**, 140.
14 J.K. Kim, *CrystEngcomm*, 2014, **16**, 2818.
15 J. Wang, J. Yang, Y. Tang, J. Liu, Y. Zhang, G. Liang, M. Gauthier, Y.C. Chen-Wiegart, M. Norouzi Banis, X. Li, R. Li, J. Wang, T.K. Sham, X. Sun, *Nat. Commun.*, 2014, **5**, 3415.
16 M.R. Yang, W.H. Ke, S.H. Wu, *J. Power Sources*, 2005, **146**, 539.
17 Z. Tan, X.Y. Wang, H.H. Zhou, *Electrochim. Acta*, 2013, **90**, 597.
18 Y.K. Sun, S.M. Oh, H.K. Park, B. Scrosati, *Adv. Mater.*, 2011, **23**, 5050.
19 R. Dominko, M. Bele, M. Gaberscek, M. Remskar, D. Hanzel, J.M. Goupil, S. Pejovnik, J. Jamnik, *J. Power Sources*, 2006, **153**, 274.
20 J.K. Kim, G.S. Chauhan, J.H. Ahn, H.J. Ahn, *J. Power Sources*, 2009, **189**, 391.
21 F. Yu, J.J. Zhang, Y.F. Yang, G.Z. Song, *J. Power Sources*, 2010, **195**, 6873.
22 P. Manikandan, P. Periasamy, R. Jagannathan, *J. Mater. Chem. A*, 2013, **1**, 15397.
23 S. Novikova, S. Yaroslavtsev, V. Rusakov, T. Kulova, A. Skundin, A. Yaroslavtsev, *Electrochim. Acta*, 2014, **122**, 180.
24 J. Chen, S. Wang, M.S. Whittingham, *J. Power Sources*, 2007, **174**, 442.
25 K. Dokko, S. Koizumi, K. Sharaishi, K. Kanamura, *J. Power Sources*, 2007, **165**, 656.
26 A. Paolella, G. Bertoni, E. Dilena, S. Marras, A. Ansaldo, L. Manna, C. George, *Nano Lett.*, 2014, **14**, 1477.
27 K. Saravanan, P. Balaya, M.V. Reddy, B.V.R. Chowdari, J.J. Vittal, *Energ Environ. Sci.*, 2010, **3**, 457.
28 M.K. Devaraju, I. Honma, *Adv. Energy Mater.*, 2012, **2**, 284.
29 Y.T. Cui, N. Xu, L.Q. Kou, M.T. Wu, L. Chen, *J. Power Sources*, 2014, **249**, 42.
30 S.W. Oh, S.T. Myung, S.M. Oh, K.H. Oh, K. Amine, B. Scrosati, Y.K. Sun, *Adv. Mater.*, 2010, **22**, 4842.
31 S.M. Oh, Y.K. Sun, *J. Power Sources*, 2013, **244**, 663.
32 D.H. Baek, J.K. Kim, Y.J. Shin, G.S. Chauhan, J.H. Ahn, K.W. Kim, *J. Power Sources*, 2009, **189**, 59.
33 D. Zhang, R. Cai, Y.K. Zhou, Z.P. Shao, X.Z. Liao, Z.F. Ma, *Electrochim. Acta*, 2010, **55**, 26531.
34 S.i. Nishimura, G. Kobayashi, K. Ohoyama, R. Kanno, M. Yashima, A. Yamada, *Nat. Mater.*, 2008, **7**, 707.
35 C. Sun, S. Rajasekhara, J.B. Goodenough, F. Zhou, *J. Am. Chem. Soc.*, 2011, **133**, 2132.
36 Y.K. Sun, S.M. Oh, H.K. Park, B. Scrosati, *Adv. Mater.*, 2011, **23**, 5050.
37 H. Liu, P. Zhang, G. C. Li, Q. Wu, Y. P. Wu, *J. Soild State Electrochem.*, 2008, **12**, 1011.
38 S.R. Das, S.B. Majumder, R.S. Katiyar, *J. Power Sources*, 2005, **139**, 261.
39 K. Tang, X. Q. Yu, J. P. Sun, H. Li, X. J. Huang, *Electrochim. Acta*, 2011, **56**, 4869.

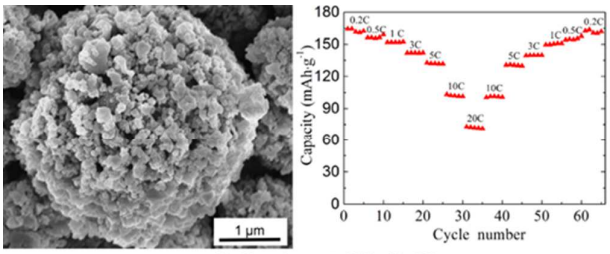

Double carbon coated $LiFe_{0.4}Mn_{0.6}PO_4$

High performance $LiFe_{0.4}Mn_{0.6}PO_4$/C microspheres cathode for lithium ion batteries was synthesized via a **double carbon coating process involved traditional techniques**